Measurement of Drug Distribution in Vascular Tissue Using Quantitative Fluorescence Microscopy

WADE K. WAN,[†,‡] MARK A. LOVICH,[†] CHAO-WEI HWANG,[†] AND ELAZER R. EDELMAN*[,†,§]

Contribution from *Harvard–MIT Division of Health Sciences and Technology, and Department of Electrical Engineering and Computer Science, Massachusetts Institute of Technology, Cambridge, Massachusetts 02139, Cardiovascular Division, Department of Medicine, Brigham and Women's Hospital, Harvard Medical School, Boston, Massachusetts 02115.*

Received September 23, 1998. Final revised manuscript received May 25, 1999.
Accepted for publication June 1, 1999.

Abstract □ Quantitative tools to assess vascular macromolecular distributions have been limited by low signal-to-noise ratios, reduced spatial resolution, postexperimental motion artifact, and the inability to provide multidimensional drug distribution profiles. Fluorescence microscopy offers the potential of identifying exogenous compounds within intact tissue by reducing autofluorescence, the process by which endogenous compounds emit energy at the same wavelength as fluorescent labels. A new technique combining fluorescence microscopy with digital postprocessing has been developed to address these limitations and is now described in detail. As a demonstration, histologic cross-sections of calf carotid arteries that had been loaded endovascularly with FITC-Dextran (20 kD) ex vivo were imaged at two different locations of the electromagnetic spectrum, one exciting only autofluorescent structures and the other exciting both autofluorescent elements and exogenous fluorescent labels. The former image was used to estimate the autofluorescence in the latter. Subtraction of the estimated autofluorescence resulted in an autofluorescence-corrected image. A standard curve, constructed from arteries that were incubated until equilibrium in different bulk phase concentrations of FITC-Dextran, was used to convert fluorescent intensities to tissue concentrations. This resulted in a concentration map with spatial resolution superior to many of the previous methods used to quantify macromolecular distributions. The transvascular concentration profiles measured by quantitative fluorescence microscopy compared favorably with those generated from the proven *en face* serial sectioning technique, validating the former. In addition, the fluorescence method demonstrated markedly increased spatial resolution. This new technique may well prove to be a valuable tool for elucidating the mechanisms of macromolecular transport, and for the rational design of drug delivery systems.

Introduction

The appeal of local pharmaceutical administration is that specific tissues and organs can be targeted for therapy without adverse systemic effects.[1−4] Yet, implementation of local delivery strategies has been limited by a whole new set of pharmacologic issues.[5] Local delivery systems impart large dynamic concentration gradients across tissues that can be difficult to identify, characterize, and control.[6] Because drug levels are not uniform, the concept of dosing takes on another level of complexity.[5] For example, cells near the point of release experience a very different concentration of drug in their extracellular milieu than do cells far away, and these levels are not static in time. The dose a cell sees depends on both time and space as well as administered drug mass. Thus, the successful implementation of local drug delivery systems requires accurate, high resolution techniques to assess drug deposition, and as proof that therapeutic levels are achieved rapidly and persist long enough for biologic effect to emerge. These very issues are especially important in considering the potential of local vascular drug therapy. The scale of the blood vessel wall dimensions, the importance and prevalence of vascular diseases, and the promise of increasingly novel vasoactive compounds make for quantification of local administration all the more essential.

We now describe the development of a new method for visualizing and quantifying drug distribution in vascular tissue. This technique utilizes fluorescence microscopy with digital postprocessing[7−10] and avoids the experimental hazards and disposal costs associated with radiolabeled compounds, while providing spatial resolution superior to conventional radioactive techniques. A nonaqueous method is used to immobilize drug and prevent postexperimental diffusion of soluble molecules. Vessel cross-sections are imaged with fluorescence microscopy, and digital postprocessing algorithms are used to reduce autofluorescence, a prior obstacle to quantitative interpretation. Autofluorescence compensation is accomplished by acquiring images at two different excitation wavelengths, one consisting of only nonspecific autofluorescence and the other containing both the specific fluorescence of markers and autofluorescence.[8,9] The former image is then used to estimate the autofluorescence in the latter image. This estimated autofluorescence could then be subtracted from the latter image to yield an autofluorescence-free image containing only the signal from the fluorescent tags. Fluorescent intensities are then converted to tissue concentrations, yielding a high-resolution map of macromolecular distribution. As a demonstration, the transvascular concentration gradient of an endovascularly applied model drug, 20 kD FITC-dextrans, is measured in the calf carotid artery. This compound was chosen for its inert properties, relative availability, and similarity in size to several vasoactive growth factors. High-resolution transvascular concentration profiles provided by this technique will yield improved understanding of macromolecular transport and deposition in vascular tissue and insight into the special pharmacologic issues raised by local delivery systems.

Experimental Protocol

Calibration Standards—Calf carotid arteries were obtained from a slaughterhouse and stored on ice for no more than 2 h. The arteries were submerged in phosphate-buffered saline with

* Corresponding author. Phone: (617) 253-1569. Fax: (617) 253-2514. E-mail: eedelman@mit.edu.
† Harvard−MIT Division of Health Sciences and Technology, MIT.
‡ Department of Electrical Engineering and Computer Science, MIT.
§ Harvard Medical School.

10.1021/js9803858 CCC: $18.00
Published on Web 07/08/1999
© 1999, American Chemical Society and American Pharmaceutical Association

calcium and magnesium (PBS^{2+}; Sigma PBS Catalog no. 1000-3, 0.01 M phosphate buffer salts, 0.120 M NaCl, 0.0027 M KCl with 0.01 M $CaCl_2$ and 0.01 M $MgCl_2$ added) throughout the preparation process to prevent dehydration and maintain tissue viability. Excess fascia and fat were gently teased away using forceps and scissors prior to sectioning vessels into cylindrical segments, 8−12 mm long and 4−8 mm in diameter. These segments were placed into separate vials containing 10 mL of 20 kD dextrans labeled with fluorescein isothiocyanate (FITC-Dx, 0.006−0.007 mol FITC per mol glucose, Sigma) in PBS^{2+} at 0, 0.02, 0.05, 0.1, 0.15, 0.2, 0.25, 0.5, 1, 2, and 2.5 mg/mL. Specimens that were incubated without any FITC-Dx will be referred to as unloaded arteries. The arteries were incubated in the dark, to prevent photobleaching, for 24 h at 4 °C. This duration was determined to be sufficient for FITC-Dx to achieve chemical equilibrium between the tissue and the bulk phase by incubating arterial segments in a single bulk phase and measuring the resulting tissue concentrations after different incubation periods. The data suggest that the tissues were fully saturated in less than 24 h, supporting the claim that 24 h is sufficient to fully load arterial segments with FITC-Dx. Incubation also did not result in any tissue swelling which would cause the calibration standards to not accurately reflect the tissue specimens. In pilot studies, the thickness of the arterial media was measured from histologic cryosections prepared both on arrival from the slaughterhouse and after incubation in PBS^{2+} for 65 h. There was no statistical difference in medial thickness at time zero (459 ± 17 μm) and at 65 h (477 ± 23 μm, $n = 3$, avg ± sd), suggesting that the tissues did not swell significantly.

Drug Immobilization and Tissue Sectioning—To immobilize drug within the tissue and limit diffusion during storage and handling, tissues were snap frozen in embedding medium (OCT, Tissue-Tek) with liquid nitrogen. Specimen blocks were stored at −20 °C prior to being cut into 20-μm-thick axial cross-sections using a precooled cryostat (CM 3050, Leica). Section thickness was previously measured to vary by less than 0.5 μm between slices. Three histologic sections were taken from each tissue standard. Frozen OCT around the tissue was gently removed to facilitate mounting onto glass slides (Superfrost Plus, VWR Scientific). The histologic sections were freeze-dried in the dark at −50 °C in a lyophilizer (Labconco) for 24 h, and stored at room temperature in a dark, dry environment prior to imaging. Freeze-drying of the tissue sections ensured that the FITC-Dx was immobilized throughout subsequent storage and processing.

Image Acquisition System—The histologic sections were imaged without any mounting medium or cover slip. Diffusion of drug from its location within the blood vessel wall was significantly reduced by snap freezing, which does not require applying a liquid phase to the tissue. 24-bit color images were acquired using a CCD video camera system (Optronics) attached to a fluorescence microscope (Optiphot-2, Nikon). The system resided on a pneumatic optical table (Technical Manufacturing Corporation) to minimize vibrations. Video images were captured on a computer (Power Computing) via a frame grabber (LG-3, Scion) using a commercial imaging software package (IPLab Spectrum, Signal Analytics). The frame grabber was calibrated by displaying a test image consisting of color bars generated from the video camera system. The gain and offset of the frame grabber were adjusted to match its dynamic range (0 to 255 units for the red, green, and blue channels) to the dynamic range of the video camera system. Magnification was provided by a 10× ocular and a 10× objective, resulting in 640 by 480 pixel images with pixel dimensions of 1.326 μm by 1.326 μm. Illumination was provided by a super high-pressure mercury lamp (Nikon) which was allowed to warm for at least 2 h prior to imaging for consistent illumination. This duration was previously determined to adequately stabilize the imaging system. Ultraviolet (UV) and FITC filter sets were used to examine tissue specimens. The UV filter set consisted of an excitation filter of 330−380 nm, a dichroic filter (beam splitter) of 400 nm, and a barrier filter of 420 nm. The FITC filter set consisted of an excitation filter of 465−495 nm, a dichroic filter of 505 nm, and a barrier filter of 515−555 nm. Images of each histologic section were acquired at 0.25, 0.5, 1.0, and 2.0 s exposure times for both UV and FITC filters. The image with the maximal signal that did not contain any saturated pixels was used. In this way each section was exposed to less than 4 s at each wavelength. In pilot studies, the impact of photobleachning was found to be negligible by continuously exposing a histologic section with drug signal to the excitation beam and acquiring sequential images. No reduction in intensities was found over one minute.

Hence forth, UV and FITC images refer to images taken with the UV and FITC filter sets, respectively. The fluorescent tag used in these experiments, FITC, is maximally excited around 490 nm so UV images contain only autofluorescence and FITC images contain both autofluorescence and specific signal from the fluorescent labels.

Initial Processing—Images were acquired using 8-bit RGB (red, green, and blue) color components and converted to the HSI (hue, saturation, and intensity) color model.[11] The HSI color model decouples luminance and chrominance in an image, with the intensity image representing the luminance information, and the hue and saturation images representing the chrominance information. Both UV and FITC images were decoupled in this manner, and the hue and saturation images were discarded leaving only the intensity image (Figure 1). Intensities in these images range from 0 (absolute black) to 255 (absolute white).

Autofluorescence Compensation—Since UV images contain only autofluorescence and FITC images contain both autofluorescence and the specific signal of interest, each pixel in a UV image can be used to estimate the autofluorescence present in the corresponding pixel in the counterpart FITC image.[8,9] A 50 pixel wide region that spanned the media but excluded the adventitia and intima was defined on both the UV and FITC images of an unloaded artery. Corresponding pixels from this region of the UV and FITC images were correlated, which allows estimation of the autofluorescence component in each pixel of this region in a FITC image, using the corresponding pixel in the counterpart UV image (Figure 1). The estimated autofluorescence was subtracted from the original FITC image yielding an autofluorescence compensated FITC image that contains only the signal from fluorescent markers (Figure 1).

Conversion of Fluorescent Intensities to Tissue Concentrations—Fluorescent intensities were converted to tissue concentrations using a standard calibration curve obtained from tissue standards incubated until equilibrium in known concentrations of FITC-Dx in PBS^{2+}. A 50 pixel wide region that spanned the media, but excluded adventitia and intima, was selected from each autofluorescence corrected FITC image (three histologic sections each with one image per standard). The average fluorescent signal in this region was correlated with the bulk phase concentration of FITC-Dx that the tissue standard was incubated in.

Whereas in bulk solutions dextrans are free to access an entire unit of volume, compounds in tissue are excluded from areas by steric interactions. Thus, the fractional accessible space in which hydrophilic drugs can distribute in tissue (ϵ) must be less than one.[6] Drug in the accessible space in a tissue is in chemical equilibrium with the bulk phase, and therefore the concentration in the accessible space is known for each tissue standard. This definition of accessible space is dependent not only on the tissue examined, but also on the specific compound of interest. The fluorescent microscopy image, however, contains contributions from both accessible and nonaccessible spaces, and concentrations are detected on a per tissue volume basis. The bulk phase concentrations of tissue standards can be converted to tissue concentration by multiplying the former by the fractional space (ϵ),[12−14]

$$c_T = \epsilon c_{Bulk} \quad (1)$$

which was measured independently (see below).

Measurement of Fractional Space Available for Distribution—To measure the fractional space available for distribution in arterial media, 1 cm long segments of calf carotid arteries were incubated for 24 h to equilibrium in 10 mL of 20 kD FITC-Dx in PBS^{2+} at concentrations (c_{Bulk}) of 0.1, 0.5, 1, and 3 mg/mL. Four arteries were incubated at each concentration. Tissue concentrations in "isolated" arterial media were measured after the intima and adventitia were removed by an *en face* cryosectioning technique (see below).[15,16] The fractional space was determined from the correlation between the bulk phase and the tissue concentrations (eq 1).

En Face Cryosectioning—Carotid artery segments were removed from incubation and cut longitudinally, unfolded, placed on a microscopy slide with the intima face down and covered in OCT. A second slide was placed on top of the specimen with two 1-mm

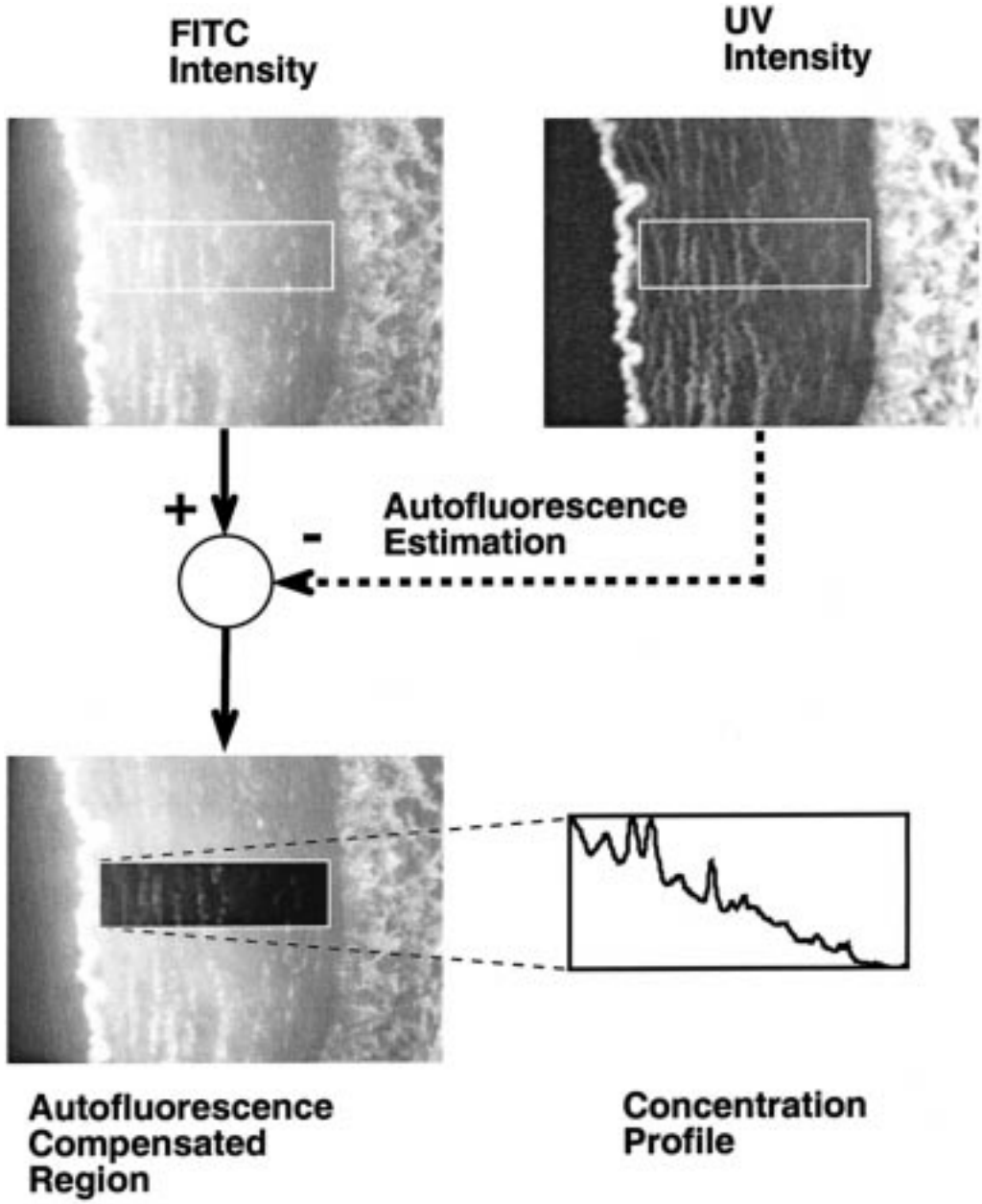

Figure 1—Image processing algorithm to compute concentration profiles. A cross-section of a calf carotid artery is imaged with the FITC and UV filter sets. A 50-pixel wide region corresponding to the media is defined from each intensity subimage. The UV region is used to estimate autofluorescence in the medial region. Pixel intensities are converted to tissue concentrations using a calibration curve. This example shows the transmedial concentration profile of fluorescent-labeled compound 2 h after endovascular application ex vivo.

spacers placed around the specimen. The glass slides were clamped together to ensure that sectioning was parallel to the intimal surface, and the tissue was snap frozen with a freezing aerosol (Cytocool II, Stephens Scientific). The frozen specimen was wrapped in aluminum foil and stored at −20° C prior to sectioning. A frozen block of OCT was mounted in the cryostat to serve as a chuck for the specimens, and was cut until the resulting surface was parallel to the blade. The cryostat was retracted so that the artery could be mounted. Arteries were separated from the slides by gently rubbing a lightly heated spatula against the slide until the specimen easily slid off. The specimens were mounted flat onto the chuck with the intima toward the blade and then trimmed into a rectangle with a razor blade. The length and width of the rectangle were measured so that the volume of each 20-μm-thick slice (V_{Slice}) could be calculated. Additional OCT was frozen around the specimen for support during sectioning.

The artery was sectioned from the intima toward the adventitia. Eighteen slices corresponding to the carotid media were pooled and reincubated in 24 mL of fresh PBS^{2+} for 48 h. This time has been shown to be more than sufficient to release more than 96% of the FITC-Dx from whole arteries. The reincubation bath volume (V_{Bath}) was more than 1000-fold greater than the volume of all the combined tissue slices, permitting the small amount of residual drug in the tissue at the end of reincubation to be neglected. The concentration of the reincubation bath was measured with a spectrofluorimeter (Fluorolog 1681, SPEX), using a standard curve of known concentrations of FITC-Dx in PBS^{2+}. This reincubation concentration ($c_{Release}$) was used to calculate the original tissue concentration of FITC-Dx in PBS^{2+} (c_T) with the following formula:

$$c_T \approx \frac{c_{Release} V_{Bath}}{n V_{Slice}} = \frac{\text{mass of released drug}}{\text{volume of tissue slices}} \quad (2)$$

where n is the number of tissue slices in each reincubation bath. Thus, the tissue concentration was measured, and the slope between the tissue and bulk phase concentrations was taken to be the fractional space of the media.[12−14] This method of measuring the fractional space assumes that binding between the compound and the tissue is insignificant.

Quantitative Fluorescence Microscopy vs *en Face* Cryosectioning—To demonstrate the validity of this technique, FITC-Dx was applied to the endovascular aspect of an artery, and the resulting transmural concentration profile was determined both through the proposed quantitative fluorescence microscopy technique and the standard method of *en face* serial cryosectioning.[15–18] Calf carotid arteries were obtained and cleaned of adventitia as described above. Arterial segments about 1.5 cm long without visible branches were cannulated at both ends and tested for leaks by visually inspecting the vessel after connecting one end to an elevated bag of Ringer's solution and closing off the other end. The intact artery was then placed in an in vitro perfusion apparatus that has been described elsewhere.[19,20] Briefly, the apparatus recirculates PBS^{2+} through the artery, simulating plasma flow, and allows control of the drug concentration in both the endovascular and perivascular compartments, which are separated by the arterial wall. 20 kD FITC-Dx (5 mg/mL) was applied to the endovascular compartment, and the continuously stirred perivascular compartment contained PBS^{2+}. Throughout this study, the hydrostatic head was set to zero, so that the transarterial pressure gradient and subsequent convective effects on molecular transport were eliminated.

Three arteries were perfused for 2 h and were then removed from the apparatus and cut in longitudinal segments, one for analysis with quantitative fluorescence microscopy, and the other with *en face* cryosectioning. Specimens for quantitative fluorescence microscopy were immediately snap frozen, sectioned onto histologic slides, freeze-dried, and imaged, as described above. Snap freezing and freeze-drying deprives the drug of an aqueous phase to diffuse and therefore significantly reduces post experimental motion artifacts. The image was autofluorescence corrected, and a 50 pixel wide region was defined which spanned the arterial media (Figure 1). The intensity values were averaged across the 50-pixel width to reduce the circumferential variance of drug distribution and were converted to FITC-Dx concentration in tissue using the standard calibration curve. Eight such transmedial regions were defined around the circumference of the artery, and their resulting transmural concentration profiles were averaged.

Specimens for *en face* cryosectioning were splayed open and frozen between two glass slides, stored, mounted, and trimmed as described above. The length and width of the opened and trimmed artery was measured with a ruler so that the volume of each 20-μm slice (V_{Slice}) could be calculated. The slices were transferred in groups of three into a 4 mL PBS^{2+} bath (V_{Bath}) and stored in the dark at 4° C for 48 h to allow drug to diffuse into the bulk phase. Three slices were used in each bath to increase the fluorescent signal into the dynamic range of the spectrofluorimeter, which was used to measure the concentration of drug in the reincubation bath ($c_{Release}$). The tissue concentration (c_T) was determined through eq 2.

Results

Autofluorescence Compensation—UV and FITC images of an unloaded artery were examined to determine the correlation between the autofluorescence with the UV and FITC filter sets. A 50-pixel wide region that spanned the arterial media was defined. The pixel intensities in this region of an UV image were linearly correlated to the corresponding intensities in the FITC image (Figure 2):

$$FITC_{autofluorescence} = 0.073UV_{total} + 44.9 \qquad (R^2 = 0.629) \quad (3)$$

The 50% confidence intervals (dashed lines) for the linear regression of eq 3 (solid line) are shown. The gray scale shading reflects the number of times data appears at the same pair of specific UV and FITC intensity values. The range of FITC values that correspond to specific UV intensities are shown in two sample histograms, which indicate limited scatter about the fitted value. This linear relationship allows the estimation of the autofluorescence component in one pixel of a FITC image using the corresponding pixel in the counterpart UV image. Assuming that

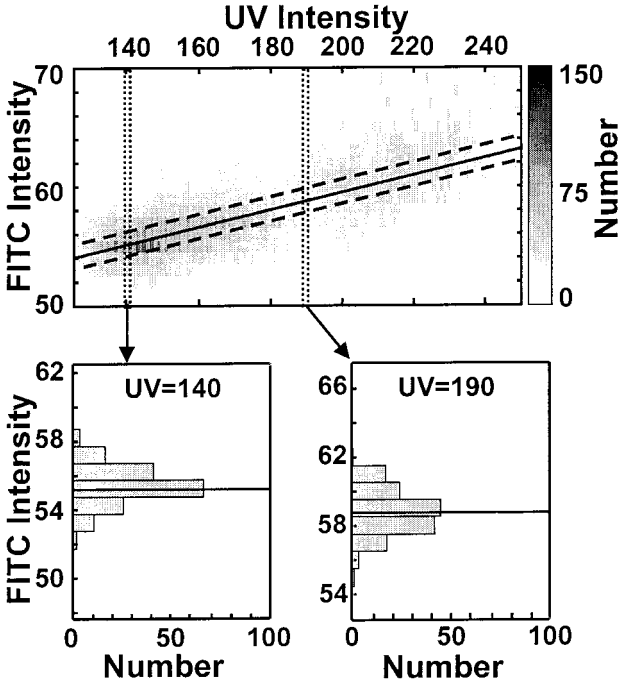

Figure 2—Correlation between autofluorescence with the UV and FITC filter sets. The media of an unloaded artery (devoid of FITC-Dx) was extracted after being imaged with the UV and FITC filter sets. Pixel intensities in the FITC image are plotted as a function of the intensity of the corresponding pixel in the counterpart UV image ($n = 9990$). The gray scale shading reflects the number of times data appears at the same pair of specific UV and FITC intensity values. The linear fit (solid line) can be used to estimate the autofluorescence in a FITC image from the corresponding UV image. The 50% confidence intervals are shown surrounding the linear fit (dashed line). Histograms are shown at two sample UV intensities and demonstrate limited scatter of FITC intensity about the fitted value.

the autofluorescence and specific fluorescence from the markers add linearly, the estimated autofluorescence can then be subtracted from the original FITC image yielding only the specific signal of fluorescent markers:

$$FITC_{specific} = FITC_{total} - FITC_{autofluorescence} = FITC_{total} - (0.073UV_{total} + 44.9) \quad (4)$$

The correlation between UV and FITC autofluorescence (eq 3) was verified by examining three other unloaded arteries subjected to the same processing. When eq 4 was used to subtract autofluorescence in histologic sections of these arteries, the resulting signal in the media hovers close to zero intensity (data not shown).

Conversion of Fluorescent Intensities to Tissue Concentrations—The conversion of fluorescent intensities to tissue concentrations requires two relations. Fluorescent intensities must first be converted to the bulk phase concentrations of tissue standards (c_{Bulk}). Three histologic axial sections were prepared and autofluorescence corrected. Regions were defined that were 50-pixel wide regions and spanned the arterial media. The mean intensity of each of these regions was fit to its corresponding bulk phase incubation concentration using a power relation (Figure 3):

$$\text{mean intensity} = 93.7c_{bulk}^{0.732} \qquad (R^2 = 0.966) \quad (5)$$

The range of this mapping is bounded by two factors. The lower concentration bound of 0.02 mg/mL is determined by the sensitivity of the image acquisition system, and low fluorescent emissions from dilute concentrations

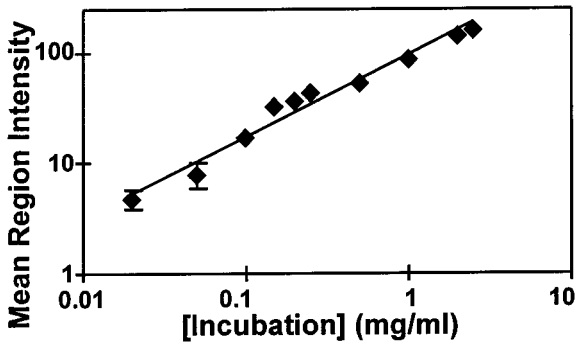

Figure 3—Fluorescent intensity as a function of incubation concentration (mean of three histologic sections from one artery ± standard deviation, $n = 3$). Tissue standards were created by incubating arteries in varying concentrations of FITC-Dx in PBS^{2+} until chemical equilibrium, and the mean intensity of a 50-pixel wide transmedial region in autofluorescence compensated images were calculated.

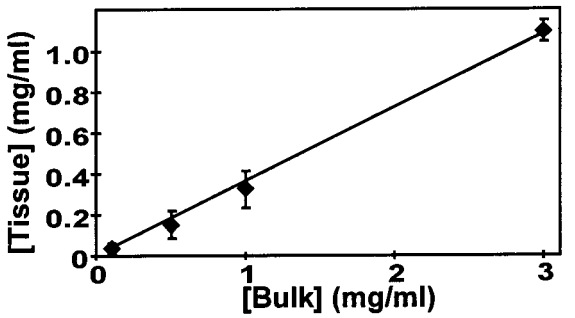

Figure 4—Tissue concentration as a function of bulk phase concentration (mean ± standard deviation, $n = 4$). Arterial segments were incubated to equilibrium in varying concentrations of FITC-Dx in PBS^{2+} until chemical equilibrium. The adventitia and intima were removed through *en face* cryosectioning, and the amount of drug in the remaining arterial media was extracted and quantified to yield the tissue concentration. The slope of the linear fit is a measure of the fractional space available for distribution in the tissue (ϵ).

of the fluorescent marker. The upper concentration bound (2.5 mg/mL) is determined by saturation of the image acquisition system. The bulk phase concentrations and the average tissue concentrations of arteries incubated to equilibrium were fit to a linear equation passing through the origin (eq 1). The slope of this line is an estimate of the fractional space accessible to the drug (ϵ). The data shows that 36.1% ($R^2 = 0.996$) of a unit volume is available for FITC-Dx distribution in the tissue (Figure 4). Equation 5 can then be rearranged and combined with eq 1:

$$c_T = \epsilon(\text{mean intensity}/93.7)^{1.37} \qquad (6)$$

This relationship was used to convert medial regions of autofluorescence corrected images from intensity to tissue concentration.

Comparison of Quantitative Fluorescence Microscopy with *en Face* Cryosectioning—Transvascular concentration profiles were obtained with the new quantitative fluorescence microscopy technique and the established method of *en face* cryosectioning (Figure 5). Three calf carotid arteries were perfused for 2 h with an endovascular bath concentration of 5 mg/mL of 20 kD FITC-Dx, a perivascular bath concentration of 0, and no transvascular pressure gradient. Each artery was cut transversely into two halves, one-half for quantitative fluorescence microscopy, the other for *en face* cryosectioning. The latter measures the average concentration in 60-μm-thick transmural divisions and this curve is depicted as a step function for one of the three arteries (Figure 5). Similar transmural

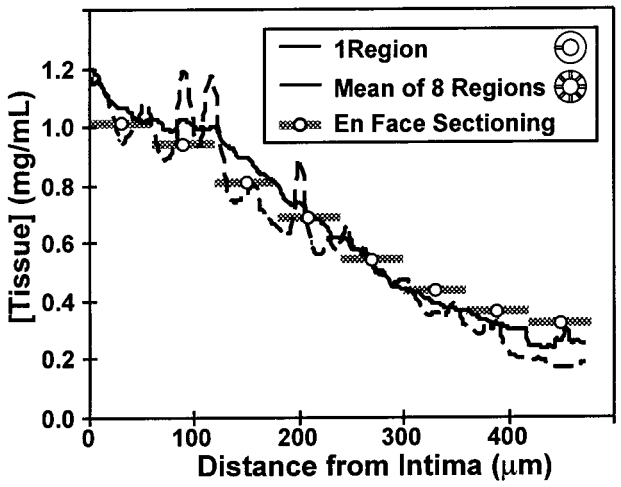

Figure 5—Transvascular concentration profiles obtained with quantitative fluorescence microscopy and *en face* cryosectioning techniques. The transmural concentration profile was obtained from a 50-pixel wide transmedial region. At each transmural location the concentration was averaged across the 50 pixels (dashed line). Another smoother transmural profile was the mean from 8 such regions, approximately equidistant around the circumference of the artery (solid line).

concentration profiles were measured for the other perfused arteries. Superimposing the profiles obtained with the two techniques demonstrates that the quantitative fluorescence microscopy technique provides higher resolution data in the form of measurements between neighboring points obtained with *en face* cryosectioning (Figure 5). For example, the quantitative fluorescence microscopy method shows peaks and valleys superimposed on a gradual transmural profile, whereas *en face* cryosectioning neglects these fine details and loses this potentially important data. Furthermore, the fluorescence technique shows a profile at a specific location about the artery and does not average the signal about the entire circumference. When transmural profiles from eight locations about the circumference of the artery are averaged, the agreement between these two methods increases (Figure 5).

Discussion

A new technique has been developed to obtain arterial concentration profiles combining fluorescence microscopy and digital image processing. Fluorescence microscopy offers several advantages over other techniques (such as higher spatial resolution and smaller marker size) that have been developed to quantify arterial concentrations of compounds, but also introduces additional limitations such as autofluorescence and the difficulty in converting fluorescent intensities to physical concentrations.

Comparison with Other Techniques—Vascular deposition studies have utilized radioactive nucleotides, which minimally change the physical structure of a compound and its transport properties, but these experiments often have limited spatial resolution and are fraught with experimental hazards and disposal costs. Early studies measured the radioactivity in grossly dissected sections providing low detection limits, but questionable repeatability as well as limited spatial resolution.[21] Measuring radioactivity in *en face* serial sections parallel to the intimal surface provides resolution down to 10 μm, but can only assess the macromolecular distribution in one direction and by necessity provides only an average concentration in the plane of sectioning.[15,16,18] The radiolabeled drug content in a specimen can also be visualized by allowing the emitted energy to expose specially prepared photographic film or a silver

emulsion applied to a histologic section.[12,22–24] Silver grain counting or optical densitometry methods can then quantify the density of exposed silver grains. These autoradiographic techniques offer increased resolution (down to ~2 μm), but may be hampered by inaccurate localization, inconsistent background radiation, and postexperimental diffusion of soluble macromolecules in the emulsion.[12,22–24] In addition, the exposure time of the film or emulsion may take months.

Nonisotopic techniques, including biochemical and fluorescent labels, offer higher spatial resolution and avoid the hazards of radioactivity, but may be limited by marker size. Large labels can affect the physicochemical and transport properties of the macromolecules under investigation. For example, the transport of horseradish peroxidase (HRP) has been quantified in arteries using a colored reaction product.[13,17,25,26] Specimens were examined with a light microscope which provided HRP concentration profiles with spatial resolution superior to radioactive techniques. Similar studies could be adapted for study of local delivery systems, however, the large size of HRP (40 kD) prevents its utility as a molecular tag on much smaller drugs. In addition, the aqueous tissue processing required to fix and embed the tissues, and to create the colored reaction product, may also allow for postexperiment diffusion of smaller or more soluble molecules. Fluorescent labels such as FITC and rhodamine isothiocyanate are smaller (~400 D), permitting their use in studies on smaller compounds. Though fluorescence microscopy offers the advantages of high spatial resolution, as in HRP studies, and smaller label size, quantitative studies have been complicated by autofluorescence and the proper application of calibration standards. This digital image processing technique seeks to address these limitations.

Autofluorescence Compensation—Constituent arterial components, such as elastin, fibronectin, and lipofuscin, exhibit autofluorescence, the emission of energy at the same wavelength as exogenous fluorescent labels.[8] The fluorescence spectra of these compounds are often very broad and autofluorescence cannot be avoided by selecting a probe with excitation and emission spectra outside their range. While uniform autofluorescence with small variability has been effectively corrected for by subtracting a constant intensity,[7,10] autofluorescent structures are often distributed inhomogeneously throughout the tissue, resulting in nonuniform artifact that is difficult to compensate for. In addition, autofluorescence may be very intense, masking the fluorescent signals of interest. Counterstaining tissue sections with solutions derived from flow cytometry such as crystal violet[27] or pontamine sky blue[28] to eliminate background autofluorescence may be impractical as aqueous processing can produce postexperimental drug diffusion. Time-resolved fluorometry, which utilizes the different decay times between autofluorescent molecules and fluorescent tags, has also been used to compensate for autofluorescence,[29,30] but utilizes a sophisticated fluorescence microscopy system and lengthy excitation times. In addition, this technique may require special fluorescent tags such as lanthanide chelates,[31] which may not be readily available individually or conjugated to compounds of interest.

Fluorescent labels have narrower excitation and emission spectra than constituent molecules of the arterial wall. Digital image processing methods have been developed that take advantage of this principle and have reduced autofluorescence, in flow cytometry studies[32] and in histologic preparations.[8,9] Images are captured at two wavelengths with one image consisting only of autofluorescence and the other image possessing both autofluorescence and the specific fluorescence signal of interest. The former image is then used to estimate the autofluorescence in the latter image. Assuming that autofluorescence and the fluorescence from the labels are simply additive, the estimated autofluorescence can be subtracted from the latter image to yield an autofluorescence-compensated image. These concepts form the basis of our quantitative fluorescence microscopy method.

Conversion of Fluorescent Intensities to Tissue Concentrations—Fluorescence microscopy is usually used as a binary tool to determine the presence or absence of a compound by qualitatively assessing the fluorescence from markers. The relation between the fluorescent intensity and tissue concentration of the tagged compound is rarely measured in histologic sections. Quantitative analysis requires the development of a reliable calibration curve to convert fluorescent intensities to physical tissue concentrations. Calibration curves have been constructed by measuring the intensity of various concentrations of FITC solution in a hemocytometer[33,34] or capillary tubes.[35] The photoabsorptive properties of solutions, however, may be very different from those of tissues. In addition, the difference in thickness of a section of tissue compared to a hemocytometer or capillary tube may cause calculated tissue concentrations to not accurately represent the actual tissue concentration.[36] Thus, calibration standards for fluorescent compounds should be created from the same substrates and conditions used in experiments and mimic the experimental samples as closely as possible to obtain reliable calibration data. In this study, this was accomplished by incubating calf carotid arteries in different concentrations until equilibrium. The transmural concentration profiles were measured in identical arteries. These calibration standards were then used to construct a relationship between fluorescent intensity and bulk phase concentration. The corresponding tissue concentration of each standard was determined through the fractional volume accessible to the compound, measured in separate experiments.

Comparison of Quantitative Fluorescence Microscopy and *en Face* Cryosectioning—The quantitative fluorescence microscopy technique described in this paper was compared to the established *en face* serial cryosectioning method (Figure 5).[15,16] This new technique performed well at predicting the complex drug distribution pattern imparted by an in vitro perfusion apparatus. Transvascular concentration profiles obtained with quantitative fluorescence microscopy have higher resolution than those obtained with *en face* cryosectioning. The resolution of the former technique is that of the light microscope, about 0.5 μm. The peaks and valleys exhibited using the technique described could not have been appreciated with en *face* cryosectioning.

The high spatial resolution of this quantitative fluorescence microscopy technique provides insights into the mechanisms of drug deposition and distribution. For example, the peaks in the tissue concentration may indicate binding or sequestration to specific arterial elements such as thin connective tissue layers. The height of these peaks are greatest in regions of increased tissue concentration and lowest away from the endovascular source of dextran, suggestive of a small degree of binding that is proportional to the local drug concentration and hence likely to be of first-order kinetics. Recent data has shown that FITC-dextran binds weakly to isolated elastin networks (data not shown). Thus, the high resolution of the quantitative fluorescence microscopy method offers insights into vascular drug deposition and distribution that could not be appreciated by traditional means.

The normalized mean square error (NMSE) between *en face* cryosectioning and the new quantitative fluorescence

microscopy technique was computed to demonstrate the statistical agreement between these two methods. The resolution of the profile from the quantitative fluorescence microscopy technique was first reduced to that of the cryosectioning profile. Data points from the profile generated with the quantitative fluorescence microscopy technique were grouped in sequential sets of 60 μm and then averaged for comparison with the cryosectioning profile. The NMSE was then computed as the sum of the squared differences between every pair of data points over the sum of the squared magnitude of every point in the cryosectioning profile. The NMSE was normalized to the cryosectioning data since cryosectioning is the standard that the new technique is being compared to. The NMSE was equal to 0.0109 for the profile obtained with one region and 0.0060 for the profile obtained by averaging across eight regions. The low NMSE demonstrates the validity and accuracy of the new fluorescence method and is not surprising given the visual similarity of the profiles in Figure 5.

There are significant differences between the transmural concentration profiles generated by quantitative fluorescence microscopy and *en face* cryosectioning (Figure 5). However, when eight concentration profiles from different locations about the circumference of a single artery generated with quantitative fluorescence microscopy were averaged, the agreement between these two methods was greatly increased. This example demonstrates that techniques such as *en face* cryosectioning, which inherently average about the circumference, gloss over important subtleties in the deposition of compounds that quantitative fluorescence microscopy can detect. Furthermore, although the potency of the fluorescence microscopy technique has been illustrated with a one-dimensional transmural concentration profile, it examines histologic sections and therefore is capable of examining drug concentration gradients in any two dimensions within a plane in which a tissue is sectioned.

Summary

This work describes a fluorescence microscopy technique to visualize and quantify drug deposition. It consists of laboratory techniques that immobilize drug in its postexperimental position, digital postprocessing to eliminate autofluorescence, and the appropriate calibration standards to convert fluorescent intensities to drug concentrations. This technique offers spatial resolution superior to conventional radioactive techniques and is adaptable to many compounds and tissues. The complex and dynamic drug deposition patterns imparted by local drug delivery systems might be defined in this manner and may ultimately allow for their rational design.

Nomenclature

c_T	Concentration of drug in a volume of tissue
c_{Bulk}	Bulk phase concentration of drug in first incubation bath
$c_{Release}$	Concentration of drug released from tissue into reincubation bath
ϵ	Fractional space in which drug can distribute through a tissue
V_{Bath}	Volume of the reincubation bath
n	Number of slices of tissue in a reincubation bath
V_{Slice}	Volume of each slice of tissue
$FITC_{Autofluorescence}$	Autofluorescence intensity of tissue imaged under FITC filter set
UV_{Total}	Autofluorescence intensity imaged under UV filter set
$FITC_{Total}$	Total intensity imaged under FITC filter set
$FITC_{Specific}$	Autofluorescence-compensated intensity under FITC filter set
FITC	Fluorescein isothiocyanate
UV	Ultraviolet

References and Notes

1. Lincoff, A. M.; Topol, E. J.; Ellis, S. G. Local Drug Delivery for the prevention of restenosis: Fact, fancy and future. *Circulation* **1994**, *90*, 2070−2084.
2. Wolinsky, H. Local Delivery: Let's keep our eyes on the wall. *J. Am. Coll. Cardiol.* **1994**, *24*, 825−827.
3. Okada, T.; Bark, D. H.; Mayberg, M. R. Local anticoagulation without systemic effect using a polymer heparin delivery system. *Stroke* **1988**, *19*, 1470−1476.
4. Edelman, E. R.; Adams, D. A.; Karnovsky, M. J. Effect of controlled adventitial heparin delivery on smooth muscle cell proliferation following endothelial injury. *Proc. Natl. Acad. Sci.* **1990**, *87*, 3773−3777.
5. Edelman, E. R.; Lovich, M. A. Drug delivery models transported to a new level. *Nature Biotechnol.* **1998**, *16*, 136−137.
6. Lovich, M. A.; Edelman, E. R. Computational simulations of local vascular heparin deposition and distribution. *Am. J. Physiol.* **1996**, *271*, H2014−H2024.
7. Sebkhi, A.; Weinberg, P. D. Effect of age on the pattern of short-term albumin uptake by the rabbit aortic wall near intercoastal branch Ostia. *Arterioscler. Thromb. Vasc. Biol.* **1996**, *16*, 317−327.
8. van de Lest, C. H. A.; Versteg, E. M. M.; Veerkamp, J. H.; van Kuppevelt, T. H. Elimination of Autofluorescence in Immunofluorescence Microscopy with Digital Image Processing. *J. Histochem. Cytochem.* **1995**, *43*, 727−730.
9. Szöllösi, J.; Lockett, S. J.; Balázs, M.; Waldman, F. M. Autofluorescence Correction for Fluorescence In Situ Hybridization. *Cytometry* **1995**, *20*, 356−361.
10. Weinberg, P. D.; Winlove, C. P.; Parker, K. H. Measurement of absolute tracer concentrations in tissue sections by using digital imaging fluorescence microscopy. Application to the study of plasma protein uptake by the arterial wall. *J. Microsc.* **1994**, *173*, 127−141.
11. Gonzalez, R. C.; Woods, R. E. *Digital Image Processing;* Addison-Wesley Publishing Company Inc.: Reading, MA, 1992; pp 229−237.
12. Fry, D. L.; Mahley, R. W.; Oh, S. Y.; Lewis, S. J.; Plowman, F.; Swyt, C. R. Quantitative microautoradiography of arteries: comparison of radioactivity to silver. *Am. J. Physiol.* **1980**, *239*, H289−H295.
13. Penn, M. S.; Saidel, G. M.; Chisolm, G. M. Vascular injury by endotoxin: changes in macromolecular transport parameters in rat aortas in vivo. *Am. J. Physiol.* **1992**, *262*, H1563−H1571.
14. Saidel, G. M.; Morris, E. D.; Chisolm, G. M. Transport of Macromolecules in Arterial Wall In Vivo: A Mathematical Model and Analytical Solutions. *Bull. Math. Biol.* **1987**, *49*, 153−169.
15. Bratzler, R. L.; Chisolm, G. M.; Colton, C. K.; Smith, K. A.; Zilversmit, D. B.; Lees, R. L. The Distribution of Labeled Albumin across the Rabbit Thoracic Aorta in Vivo. *Circ. Res.* **1977**, *40*, 182−190.
16. Bratzler, R. L.; Chisolm, G. M.; Colton, C. K.; Smith, K. A.; Lees, R. S. The Distribution of Labeled Low-Density Lipoproteins Across the Rabbit Thoracic Aorta in Vivo. *Atherosclerosis* **1977**, *28*, 289−307.
17. Penn, M. S.; Koelle, M. R.; Schwartz, S. M.; Chisolm, G. M. Visualization and Quantification of Transmural Concentration Profiles of Macromolecules Across the Arterial Wall. *Circ. Res.* **1990**, *67*, 11−22.
18. Ramirez, C.; Colton, C.; Smith, K.; Stemerman, M.; Lees, R. Transport of ^{125}I−Albumin Across Normal and Deendothelialized Rabbit Thoracic Aorta In Vivo. *Arteriosclerosis* **1984**, *4*, 283−291.
19. Lovich, M. A.; Edelman, E. R. Mechanisms of Transmural Heparin Transport in the Rat Abdominal Aorta After Local Vascular Delivery. *Circ. Res.* **1995**, *77*, 1143−1150.

20. Lovich, M. A.; Philbrook, M.; Sawyer, S.; Weselcouch, E.; Edelman, E. R. Arterial heparin deposition: role of diffusiion, convection, and extravascular space. *Am. J. Physiol.* **1998**, *275*, H2236−H2242.
21. Duncan, L. E.; Buck, K.; Lynch, A. Lipoprotein Movement through Canine Aortic Wall. *Science* **1963**, *142*, 972−973.
22. Aitken, W. M.; Wright, E.; Gray, H. S. Autoradiography of Water-Diffusible Substances in Sections of Whole Baby Rats. *Stain Technol.* **1968**, *43*, 1−7.
23. Schnitzer, J. J.; Morrel, E. M.; Colton, C. K.; Smith, K. A.; Stemerman, M. B. Absolute Quantitative Autoradiography of Low Concentrations of [^{125}I]-Labeled Proteins in Arterial Tissue. *J. Histochem. Cytochem.* **1987**, *35*, 1439−1450.
24. Tompkins, R. G.; Yarmush, M. L.; Schnitzer, J. J.; Colton, C. K.; Smith, K. A.; Stemerman, M. B. Low-density lipoprotein transport in blood vessel walls of squirrel monkeys. *Am. J. Physiol.* **1989**, *257*, H452−H464.
25. Penn, M. S.; Chisolm, G. M. Relation Between Lipopolysaccharide-Induced Endothelial Cell Injury and Entry of Macromolecules Into the Rat Aorta In Vivo. *Circ. Res.* **1991**, *68*, 1259−1269.
26. Penn, M. S.; Saidel, G. M.; Chisolm, G. M. Relative Significance of Endothelium and Internal Elastic Lamina in Regulating the Entry of Macromolecules Into Arteries In Vivo. *Circ. Res.* **1994**, *74*, 74−82.
27. Halldén, G.; Sköld, C. M.; Eklund, A.; Forslid, J.; Hed, J. Quenching of intracellular autofluorescence in alveolar macrophages permits analysis of fluorochrome labeled surface antigens by flow cytofluorometry. *J. Immunol. Methods* **1991**, *142*, 207−214.
28. Cowen, T.; Haven, A. J.; Burnstock, G. Pontamine sky blue: A counterstain for background autofluorescence in fluorescence and immunofluorescence histochemistry. *Histochemistry* **1985**, *82*, 205−208.
29. Koppel, D. E.; Carlson, C.; Smilowitz, H. Analysis of heterogeneous fluorescence photobleaching by video kinetics imaging: the method of cumulants. *J. Microsc.* **1989**, *155*, 199−206.
30. Marriott, G.; Clegg, R. M.; Arndt-Jovin, D. J.; Jovin, T. M. Time-resolved imaging microscopy: Phosphorescence and delayed fluorescence imaging. *Biophys. J.* **1991**, *60*, 1374−1387.
31. Seveus, L.; Väisälä, M.; Syrjänen, S.; Sandberg, M.; Kuusisto, A.; Harju, R.; Salo, J.; Hemmilä, I.; Kojola, H.; Soini, E. Time-Resolved Fluorescence Imaging of Europium Chelate Label in Immunohistochemistry and In Situ Hybridization. *Cytometry* **1992**, *13*, 329−338.
32. Steinkamp, J. A.; Stewart, C. C. Dual-Laser, Differential Fluorescence Correction Method for Reducing Cellular Background Autofluorescence. *Cytometry* **1986**, *7*, 566−574.
33. Nakamura, Y.; Wayland, H. Macromolecular Transport in the Cat Mesentery. *Microvasc. Res.* **1975**, *9*, 1−21.
34. Fox, J. R.; Wayland, H. Interstitial Diffusion of Macromolecules in the Rat Mesentery. *Microvasc. Res.* **1979**, *18*, 255−276.
35. Nugent, L. J.; Jain, R. K. Plasma pharmacokinetics and interstitial diffusion of macromolecules in a capillary bed. *Am. J. Physiol.* **1984**, *246*, H129−H137.
36. Armenante, P. M.; Kim, D.; Duran, W. N. Experimental Determination of the Linear Correlation between in Vivo TV Fluorescence Intensity and Vascular and Tissue FITC-DX Concentrations. *Microvasc. Res.* **1991**, *42*, 198−208.

Acknowledgments

This study is supported in part by grants from the National Institutes of Health (GM/HL 49039), the Burroughs-Welcome Fund in Experimental Therapeutics, and the Whitaker Foundation in Biomedical Engineering. Elazer R. Edelman is an Established Investigator of the American Heart Association. The authors acknowledge the technical assistance of Lily Y. Chen and expert advice of Philip Seifert and Dr. David Ettenson.

JS9803858